Bioactive Materials 18 (2022) 91–103

Contents lists available at ScienceDirect

Bioactive Materials

journal homepage: www.keaipublishing.com/en/journals/bioactive-materials

Upconversion nanoparticles regulated drug & gas dual-effective nanoplatform for the targeting cooperated therapy of thrombus and anticoagulation

Shichen Liu [a,b], Yao Sun [b], Teng Zhang [a,b], Longtao Cao [b], Zhiwei Zhong [a], Haoxin Cheng [b,c], Qingqing Wang [b], Zhuang Qiu [b,d], Weimin Zhou [a,**], Xiaolei Wang [b,c,*]

[a] Department of Vascular Surgery, The Second Affiliated Hospital of Nanchang University, Nanchang University, Nanchang, Jiangxi, 330006, PR China
[b] The National Engineering Research Center for Bioengineering Drugs and the Technologies, Institute of Translational Medicine, Nanchang University, Nanchang, Jiangxi, 330088, PR China
[c] College of Chemistry, Nanchang University, Nanchang, Jiangxi, 330088, PR China
[d] School of Public Health & Jiangxi Provincial Key Laboratory of Preventive Medicine, Nanchang, Jiangxi, 330088, PR China

ARTICLE INFO

Keywords:
Targeted drug delivery
Upconversion nanoparticles
Controlled release
Thrombus
Anticoagulation

ABSTRACT

Thromboembolism is the leading cause of cardiovascular mortality. Currently, for the lack of targeting, short half-life, low bioavailability and high bleeding risk of the classical thrombolytic drugs, pharmacological thrombolysis is usually a slow process based on micro-pumping. In addition, frequently monitoring and regulating coagulation functions are also required during (and after) the process of thrombolysis. To address these issues, a targeted thrombolytic and anticoagulation nanoplatform (UCATS-UK) is developed based on upconversion nanoparticles (UCNPs) that can convert 808 or 980 nm near-infrared (NIR) light into UV/blue light. This nanoplatform can target and enrich in the thrombus site. Synergistic thrombolysis and anticoagulation therapy thus could be realized through the controlled release of urokinase (UK) and nitric oxide (NO). Both *in vitro* and *in vivo* experiments have confirmed the excellent thrombolytic and anticoagulative capabilities of this multifunctional nanoplatform. Combined with the unique fluorescent imaging capability of UCNPs, this work is expected to contribute to the development of clinical thrombolysis therapy towards an integrated system of imaging, diagnosis and treatment.

1. Introduction

Thromboembolism is the leading cause of cardiovascular mortality, and its high incidence has placed a serious socio-economic burden [1–7]. Generally, patients prefer to receive systemic thrombolytic therapy with thrombolytic drugs represented by urokinase (UK) than invasive surgical retrieval. However, due to the short half-life (9–12 min) and low bioavailability of UK, repeated dosing is usually required, but overdose has the potential to damage the blood-brain barrier and thus causing fatal intracranial haemorrhage [8,9]. Clinically, UK is usually micro-pumped into patients for thrombolytic therapy in accompany with frequent coagulation monitoring, which undoubtedly increases the pain and expenses of patients. In addition, the recurrence rate of thrombus within 12 months after thrombolytic therapy is about 5–10%, thus anticoagulation after thrombolysis is equally essential [3,10–12]. Nevertheless, long-term use of anticoagulant drugs also increases the risk of major bleeding [13,14]. Currently, the nanomaterials are widely used in diagnosis and treatment [15–18], in view of the foundation of prior work in thrombus therapy [19–25], we hope to construct a nanoplatform with integrated targeted thrombolytic and anticoagulant capabilities, *i.e.*, after a single injection, the nanoplatform can target to the thrombus site followed by a sustained and controlled release of UK and is supplemented with drug-free anticoagulation therapy, so as to reduce the risk of bleeding.

Peer review under responsibility of KeAi Communications Co., Ltd.
* Corresponding author. The National Engineering Research Center for Bioengineering Drugs and the Technologies, Institute of Translational Medicine, Nanchang University, Nanchang, Jiangxi, 330088, PR China.
** Corresponding author.
E-mail addresses: zwmsubmit@126.com (W. Zhou), wangxiaolei@ncu.edu.cn (X. Wang).

https://doi.org/10.1016/j.bioactmat.2022.03.013
Received 17 November 2021; Received in revised form 9 March 2022; Accepted 9 March 2022
Available online 17 March 2022

Controlled release of UK can increase drug utilization and reduce side effects, and our group previous work has achieved controlled release of UK through photothermal regulation [26]. Compared with utilizing temperature to control drug release, light-controlled drug or gas release based on more energetic UV or visible light is theoretically a more precise and efficient method [27–29]. However, the biological applications of UV and visible light are limited by the depth of penetration [30]. To address this problem, we introduced the rare earth-doped upconversion nanoparticles (UCNPs) into thrombus therapy, where the UCNPs can convert near-infrared light (NIR) with biological tissue penetration into more energetic UV and visible light [28, 31–35]. Azobenzene (azo) can be reversibly isomerized between cis and trans under visible and UV light irradiation, thus can act as a photo-responsive impeller for desirable light-controlled drug release [36–38]. In this study, the light-controlled drug release nanocarriers (UCNP@$mSiO_2$-azo, UCA) were constructed by coating mesoporous silica on the surface of UCNPs (UCNP@$mSiO_2$, UCM) and installing photomechanical azo inside the mesopores.

Apart from reliable light-controlled drug release, how to integrate both targeting and anticoagulative capabilities into the nanocarriers is another major challenge in this work. To address this requirement, we modified the surface of nanocarriers with nitric oxide donor (SNAP) and platelet targeting molecule (tirofiban) to obtain a multifunctional nanoplatform UCNP@$mSiO_2$-azo-Tirofiban-SNAP (UCATS) with targeted thrombolytic and anticoagulative capabilities. On the one hand, tirofiban is a non-peptide platelet glycoprotein IIb/IIIa (GPIIb/IIIa) receptor antagonist with an RGD-like structure, which can target to the GPIIb/IIIa receptor on the platelet surface [39–41]. On the other hand, S-nitroso-N-acetyl-DL-penicillamine (SNAP), as one of the most stable nitrosothiol species, is able to absorb UV light to release nitric oxide (NO) with anticoagulative effects [42–45]. As shown in Scheme 1, when thrombosis occurs, the surface modified tirofiban on the nanoplatform can guide the nanoparticles target and enrich at the thrombus site. Under the NIR light irradiation, the UCNPs can convert NIR light to UV and blue light, which can fuel azo to propel the UK release at the thrombus site controllably, thus performing thrombolytic effect and minimizing the bleeding side effects caused by overuse of UK. Meanwhile, the NIR-triggered release of NO can decrease the intracytoplasmic Ca^{2+} concentration of platelets, thereby inhibiting platelet activation and aggregation, exerting anticoagulative effect and prevent thrombus recurrence without increasing the risk of bleeding.

2. Materials and methods

2.1. Materials

Yttrium (III) acetate hydrate ($Y(CH_3CO_2)_3{\cdot}xH_2O$, 99.9%), ytterbium (III) acetate hydrate ($Yb(CH_3CO_2)_3{\cdot}xH_2O$, 99.95%), thulium (III) acetate hydrate ($Tm(CH_3CO_2)_3{\cdot}xH_2O$, 99.9%), neodymium (III) acetate hydrate ($Nd(CH_3CO_2)_3{\cdot}xH_2O$, 99.9%), 1-octadecene (ODE, tech grade, 90.0%), oleic acid (OA, tech grade, 90.0%), 4-phenylazobenzoyl chloride (97.0%), tirofiban (≥98.5%) and S-nitroso-N-acetyl-DL-penicillamine (SNAP, ≥ 97.0%) were purchased from Sigma Co., LTD. Ammonium fluoride (NH_4F, 98.0%) and tetraethyl orthosilicate (TEOS, 99.0%) were purchased from Alfa Co., LTD. DAF-FM DA and Hoechst 33342 were purchased from MCE Co., LTD. 4-(4,6-dimethoxy-1,3,5-triazin-2-yl)-4-methylmorpholinium chloride (DMTMM, 97.0%) was purchased from J&K Scientific. Nitric Oxide Assay Kit was purchased from Solarbio Co., LTD. Urokinase ELISA Kit was purchased from Keshun Science and Technology Co., LTD. (3-aminopropyl) triethoxysilane (APTES, 99.0%)

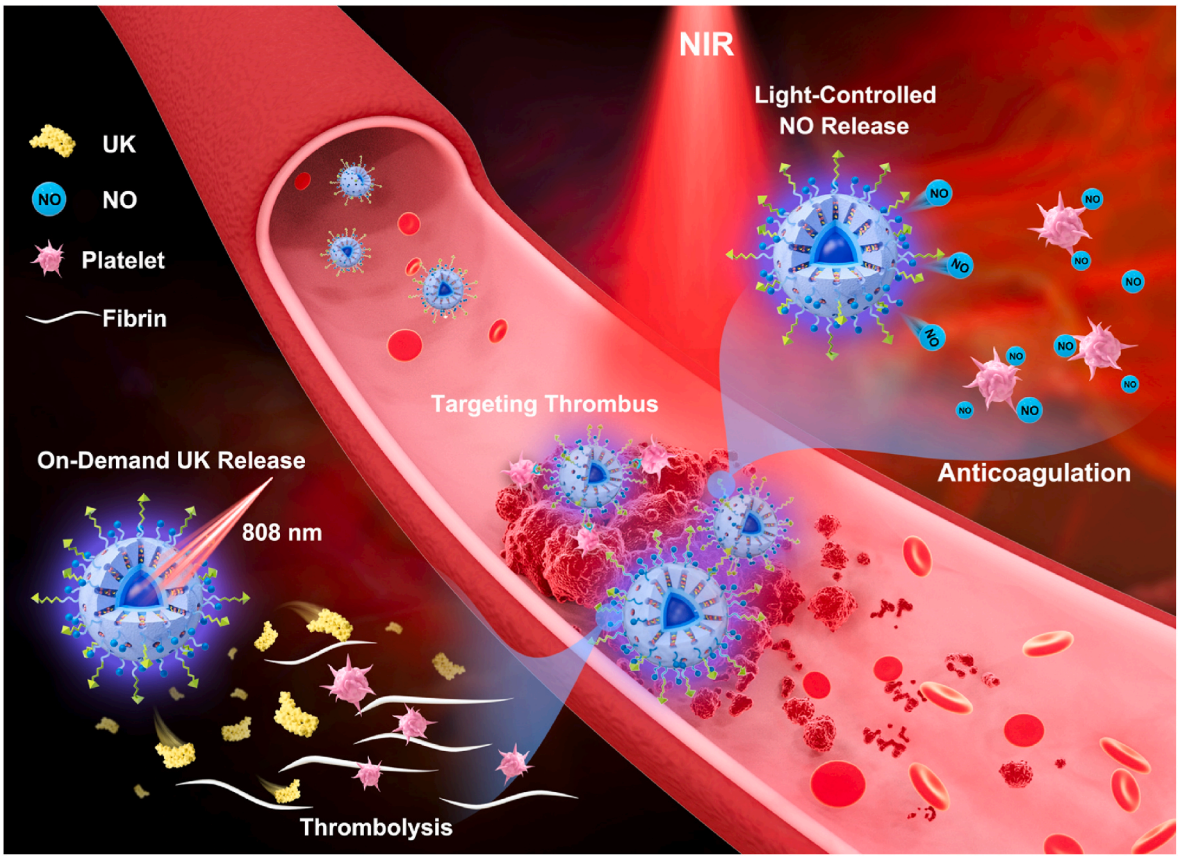

Scheme 1. Schematic illustration of NIR controlled release of UK and NO from UCATS-UK for targeting thrombolysis and anticoagulation therapy. The UCATS-UK can target on the thrombus site and emitted UV/blue light under 808 nm NIR irradiation. Meanwhile, The UCL can fuel azobenzene to propel the UK on-demand release as well as excited NO release for synergistic thrombolysis and anticoagulation therapy.

was purchased from Aladdin Co., Ltd. Urokinase (UK, 100000 IU mg^{-1}), plasminogen (≥2.0 units mg^{-1}), triethylamine (≥99.5%), hexadecyl trimethyl ammonium bromide (CTAB, 99.0%), sodium hydroxide (NaOH, 97.0%), sodium chloride (NaCl, 99.5%) and sodium nitrite ($NaNO_2$, 99.9%) were purchased from Macklin Co., Ltd. Methanol. Ethanol and cyclohexane were purchased from Xilong Science Co., LTD. Coagulation factor Ⅶ and Coagulation factor Ⅸ ELISA Kits were purchased from Camilo Biological Co., LTD. All chemicals were used without further purification.

2.2. Synthesis of β-$NaYF_4$:Yb,Tm nanocrystals

The core nanocrystals of $NaYF_4$:20%Yb,0.5%Tm were synthesized by thermal decomposition method with slightly modified [46]. Briefly, 0.795 mmol of $Y(CH_3CO_2)_3$, 0.2 mmol of $Yb(CH_3CO_2)_3$ and 0.005 mmol of $Tm(CH_3CO_2)_3$ were added into a 50 mL three-necked flask containing 6 mL of OA and 15 mL of 1-octadecene. The mixture was heated to 150 °C to obtain a transparent solution. After that, the solution was cooled down to room temperature. Then 10 mL methanol containing 4 mmol of NH_4F and 2.5 mmol of NaOH was added and stirred for 30 min at 50 °C. After methanol had evaporated, the solution was heated to 300 °C and maintained for 1.5 h under argon protection. The resulting nanoparticles were precipitated by the addition of ethanol, collected by centrifugation at 10000 rpm for 10 min, washed with cyclohexane and ethanol for three times, and finally redispersed in cyclohexane.

2.3. Synthesis of Core@Shell UCNP nanocrystals

The transparent solution was obtained by adding 0.4 mmol of $Y(CH_3CO_2)_3$ and 0.1 mmol of $Nd(CH_3CO_2)_3$ into a 50 mL three-necked flask containing 3 mL OA and 7.5 mL 1-octadecene, respectively, and heating to 150 °C. After that, the solution was cooled down to room temperature. Then the obtained core nanocrystals in cyclohexane and 5 mL methanol containing 2 mmol of NH_4F and 1.25 mmol of NaOH was added and stirred for 30 min at 50 °C. After methanol had evaporated, the solution was heated to 300 °C and maintained for 1.5 h under argon protection. The resulting nanoparticles were precipitated by the addition of ethanol, collected by centrifugation at 10000 rpm for 10 min, washed with cyclohexane and ethanol for three times, and finally redispersed in cyclohexane.

2.4. Synthesis of Core@Shell@Shell UCNP nanocrystals

The synthesis was carried out exactly as outlined for $NaYF_4$:Nd shell growth mentioned above. 0.5 mmol of $Y(CH_3CO_2)_3$ was added into a 50 mL three-necked flask containing 3 mL OA and 7.5 mL 1-octadecene and heating to 150 °C. After that, the solution was cooled down to room temperature. Then the obtained core@shell nanocrystals in cyclohexane and 5 mL methanol containing 2 mmol of NH_4F and 1.25 mmol of NaOH was added and stirred for 30 min at 50 °C. After methanol had evaporated, the solution was heated to 300 °C and maintained for 1.5 h under argon protection. The synthesized core@shell@shell upconversion nanoparticles were precipitated by the addition of ethanol, collected by centrifugation at 10000 rpm for 10 min, washed with cyclohexane and ethanol for three times, and finally redispersed in cyclohexane.

2.5. Synthesis of selective surface amino-functionalized UCNP@$mSiO_2$ nanoparticles

CTAB (0.1 g) was dissolved in 25 mL water and heated to 80 °C under stirring. Then 1 mL UCNPs cyclohexane solution (10 mg mL^{-1}) was added, and after evaporation of the cyclohexane, 25 mL of deionized water containing 5 mL of ethanol was added. When the temperature of the mixture was stabilized at 70 °C, 100 μL NaOH (2 M) was poured in and 100 μL TEOS was added dropwise under vigorous stirring for 30 min. After that, 5 μL APTES was added and stirred for 6 h to modify the amino group on the outer surface of UCNP@$mSiO_2$ (UCM). The as-synthesized UCNP@$mSiO_2$-NH_2 (UCM-NH_2) nanoparticles were collected and washed with ethanol for three times. To remove the template CTAB, UCM-NH_2 was extracted with 1 wt% NaCl methanol solution for three times. The product was obtained by washing with ethanol and water for several times, and dried under vacuum.

2.6. Synthesis of UCNP@$mSiO_2$-azo-Tirofiban-SNAP

First, the UCNP@$mSiO_2$-azo (UCA) was synthesized as a formerly reported way [36]. 10 mg UCM-NH_2 was added into a solution containing 10 mL ethanol and 80 mg N-(3-triethoxysilyl) propyl-4-phenylazobenzamide. Then the mixture was heated to 80 °C and stirred for 1 h. The synthesized UCA was collected by centrifugation and washed with ethanol and water for three times. For conjunction of tirofiban and SNAP, different molar ratios of SNAP and tirofiban (total 0.02 mmol) were dissolved in 5 mL phosphate buffer saline (PBS, 0.1 M, pH 8.0), and then 7.5 mg DMTMM was added into the solution and stirred for 15 min at room temperature. After that, 5 mg UCA was dispersed in the mixture and stirred for 8 h in dark condition for conjugation of tirofiban and SNAP on the surface of UCA. The modification rate was measured according to the standard curves of SNAP and tirofiban. The modification rate was calculated as follow equation:

$$\text{Modification rate} = \frac{\text{Weight of modificated SNAP or tirofiban}}{\text{Weight of UCATS}} \times 100\%$$

The functionalized UCNP@$mSiO_2$-azo-Tirofiban-SNAP (UCATS) was collected by centrifugation, washed with PBS for three times, and stored at 4 °C for later use.

2.7. Preparations of UK loaded UCATS (UCATS-UK)

UCATS (5 mg) was uniformly dispersed in 5 mL PBS solution containing 1 mg urokinase and stirred overnight at room temperature in dark conditions. The as-prepared UCATS-UK was collected by centrifugation at 10000 rpm for 15 min and stored at 4 °C.

2.8. Characterization

The morphology of the as-synthesized nanoparticles was observed using field-emission transmission electron microscopes (TEM, Tecnai G2 20, Thermo, US) and field-emission scanning electron microscopy (SEM, ZEISS Sigma 300, England). X-ray diffraction (XRD) pattern was recorded by a D8A A25 X (Bruker, Germany). Fourier transform infrared (FT-IR) spectroscopy was performed on Nicolet iS20 (Thermo, US). Zeta potentials of samples were determined by a Zetasizer Nano ZS90 (Malvern, UK). The UCL spectra were measured by a fluorescence spectrophotometer (FL970, Techcomp, China). Nitrogen adsorption-desorption isotherms were obtained by an Autosor-iQ (Quantanchrome INSTRUMENTS, US). The Brunauer-Emmett-Teller (BET) method was utilized to calculate the specific surface area by using adsorption data in the range of the relative pressures from 0.01 to 1.00. The pore-size distributions were calculated using the Barrett-Joyner-Halanda (BJH) method. The thermogravimetric (TG) analysis was performed on TGA 4000 (PE, US). The inductively coupled plasma optical emission spectrometry (ICP-OES) was determined by Optima 8000 (PerkinElmer, US). The UV–vis absorption data were collected by UV-2600 spectrophotometer (SHIMADZU, Japan). The platelet aggregation was analyzed by automatic platelet aggregator (AG800, Techlink, China). The H&E staining and stained cells were analyzed using microscope (Olympus, Japan) and inverted fluorescence microscopy (Olympus, Japan). The absorbance of Cell Counting Kit 8 (CCK-8) was measured by the microplate reader of VICTOR Nivo 3S (PerkinElmer, UK). SLA 3D printer (Pegasus Touch, USA) was used to print the simulated vein vasculature. The *in vivo* fluorescence imaging was recorded by IVIS Lumina XR III (Perkin elmer, US). The *in vivo* ultrasound imaging was recorded by

VINNO 6 (VINNO, China).

2.9. NIR-triggered UK release

To evaluate the light-controlled UK release, 5 mg UCATS-UK was dispersed in 5 mL PBS buffer and exposed under 808 nm NIR with different power densities (0, 1 and 2 W cm^{-2}). The UCATS-UK was exposed to intermittent 808 nm NIR for 3 h (exposure for 10 min, stop for 10 min, and then exposure for 10 min again). Then, the supernatant was collected every 10 min to measure the release of UK by Urokinase ELISA Kit.

2.10. NIR-responsive NO release detection

Different concentrations of UCATS (0, 500 μg mL^{-1} and 1 mg mL^{-1}) and SNAP (200 μg mL^{-1}) solutions were prepared. Then the samples were irradiated by 2 W cm^{-2} 808 nm NIR. The NO release from UCATS (1 mg mL^{-1}) under different power densities of 808 nm NIR (0, 0.5, 1 and 2 W cm^{-2}) irradiation was also performed. After each 10 min, the supernatant was collected to measure the concentration of released NO by Nitric Oxide Assay Kit. By measuring the optical density (OD) at 550 nm, the released concentration of NO was calculated according to the standard curve of $NaNO_2$.

2.11. Intracellular NO release detection

The NO probe DAF-FM DA was used for detecting the NIR-triggered NO release in cells. Human umbilical vein endothelial cells (HUVECs) were seeded in 24-well plates at 2×10^5 cells per well and cultured with Roswell Park Memorial Institute (RPMI) 1640 medium containing 10% fetal bovine serum, 100 U mL^{-1} of penicillin and 100 μg mL^{-1} streptomycin at 37 °C under 5% CO_2 atmosphere. After HUVECs were adherent, the HUVECs were treated with the DAF-FM DA solution (5 μM) at 37 °C for 1 h. After that, the UCATS was added and incubated with HUVECs for 2 h, then exposed to 808 nm NIR for 10 min (1 W cm^{-2}). Finally, the Hoechst 33342 was added for nuclei staining. The stained HUVECs were analyzed using inverted fluorescence microscopy.

2.12. Preparation of thrombus

After Sprague-Dawley (SD) rats were anesthetized with isoflurane, fresh blood was collected. Then 100 μL fresh blood was added into a tube contained 10 μL thrombin (25 U mL^{-1}) and placed at 37 °C for 3 h to form a thrombus.

2.13. Static thrombolysis evaluation in vitro

The thrombus was prepared and placed into a transparent bottle containing 3 mL of different sample solutions (0.5 mg mL^{-1}) and 50 μg plasminogen, among them, the UK group was added equivalent amount of loaded UK in UCTAS-UK (about 100 μg). Then, the thrombus was taken out and weighed at setting time. The groups requiring NIR irradiation were exposed under 2 W cm^{-2} 808 nm NIR for 10 min per hour. After that, the OD_{415} of the supernatant in each group was detected as indicator of fibrin.

2.14. Dynamic thrombolysis evaluation in vitro

Briefly, simulated vein vasculature models were printed by 3D printer. Different samples (0.5 mg mL^{-1}) and 50 μg plasminogen dispersed in 3 mL saline were added into the 3D vein vasculature models, among them, the native UK group was added equivalent amount of loaded UK in UCTAS-UK (about 100 μg). The constant flow pump was used to simulate blood flow and the blood flow rate was 60 mL min^{-1}. The prepared thrombus was placed and blocked in the vein vasculature models, and the weight of the thrombus was recorded at setting time.

2.15. Platelet aggregation assays

The blood samples were collected from rats. The blood samples were centrifuged at 850 rpm for 10 min at room temperature to collect the platelet rich plasma. The obtained platelet was treated with different samples (200 μg mL^{-1}). Among them, the tirofiban group and SNAP group were added equivalent dose of the modified tirofiban and SNAP in UCTAS. Then, the groups requiring NIR irradiation were exposed under 2 W cm^{-2} 808 nm NIR for 10 min. After that, each group was mixed with platelet activator adenosine diphosphate (ADP) and analyzed for platelet aggregation by using an automatic platelet aggregator (AG800).

2.16. In vitro platelet targeting assay

The platelet targeting assay was performed to verify the platelet targeting ability of UCATS [47]. The platelet rich plasma was centrifuged at 3500 rpm for 10 min to collect platelets and washed with Tyrode's solution. Then, the collected platelets were added with 100 μL of 10 μM ADP or 100 μL saline to obtain activated and non-activated platelets, respectively. The activated and non-activated platelets were incubated with 200 μg mL^{-1} UCATS for 1 h, respectively. After that, the platelets were washed with Tyrode's solution and then digested to measure the concentration of Nd^{3+} by ICP-OES.

2.17. Cytotoxicity test

The viability of HUVECs and mouse fibroblasts cell (L929) were purchased from Mingzhou Bio. Co., LTD. (Ningbo, China) and the viabilities of HUVECs and L929 were evaluated by CCK-8 assay. The cells were seeded in 96-well plates at 2×10^3 cells per well and cultured with RPMI 1640 medium containing 10% fetal bovine serum, 100 U mL^{-1} of penicillin and 100 μg mL^{-1} streptomycin at 37 °C under 5% CO_2 atmosphere for 12 h. After the cells were adherent, medium containing UCATS at different concentrations was added and co-cultured for 24, 48 and 72 h. Besides, the HUVECs requiring NIR irradiation were irradiated with 2 W cm^{-2} 808 nm NIR for 10 min. After a certain period of time, the medium was changed to the medium containing 10% CCK-8 and cultured for 2 h. The absorbance was determined using a microplate reader at a wavelength of 450 nm. The cell viability (%) was calculated as follows:

$$\text{Cell viability} = \frac{(OD_e - OD_b)}{(OD_c - OD_b)} \times 100\%$$

where OD_e represents the OD value of the experimental groups, OD_b represents the OD value of the blank group, and OD_c represents the OD value of the control group.

2.18. Cell live/dead staining

The HUVECs and L929 cells were seeded in 24-well plates at 2×10^5 cells per well and cultured with RPMI 1640 medium containing 10% fetal bovine serum, 100 U mL^{-1} of penicillin and 100 μg mL^{-1} streptomycin at 37 °C under 5% CO_2 atmosphere for 12 h. After the cells were adherent, medium containing UCATS at different concentrations was added and co-cultured for 24 h. Then Calcein-AM and PI stains were added and viewed by inverted fluorescent microscope.

2.19. Hemolysis assay

The red blood cells (RBCs) were isolated from SD rats, cleaned and diluted with 0.9% NaCl solution. Subsequently, 100 μL diluted RBCs were added to 0.9% NaCl solution (1.1 mL) as negative control and 100 μL diluted RBCs were added to deionized water (1.1 mL) as positive control, respectively. In the experimental groups, 100 μL diluted RBCs were mixed with 100 μL UCATS at different concentrations and 0.9%

NaCl solution (1.0 mL), respectively. The absorbance of the supernatant at 540 nm was determined after 2 h water bath at 37 °C. The hemolysis rate of each group was calculated as follows:

$$\text{Hemolysis rate} = \frac{(OD_0 - OD_1)}{(OD_2 - OD_1)} \times 100\%$$

where OD_0 represents the OD value of the experimental groups, OD_1 represents the OD value of the negative control group, and OD_2 represents the OD value of the positive control group.

2.20. In vitro and in vivo photothermal effect assay

Briefly, 5 mL PBS was placed in the glass bottle and exposed under continuous 2 W cm^{-2} 808 nm or 980 nm NIR irradiation for 10 min. Thermal images and temperatures were captured and recorded at setting time points. For *in vitro* photothermal effect, HUVECs were seeded in 24-well plates at 2×10^5 cells per well and cultured for 12 h. Then, the above cells were irradiated with 2 W cm^{-2} 808 nm or 980 nm NIR for 10 min. After adding Calcein-AM and PI staining, the cells were observed with an inverted fluorescence microscope. For *in vivo* photothermal effect, the SD rats were anesthetized and exposed under 2 W cm^{-2} 808 nm or 980 nm NIR. Thermal images and temperatures were captured and recorded at different time points.

2.21. In vivo thrombus targeting

All experiments were conducted in accordance with the guidelines and approved by the ethics committee of Nanchang University (Nanchang, China, SYXK 2018-0006). The male SD rats (4 weeks old) were randomly divided. Then, the inferior vena cava thrombus models were constructed, and different samples (5 mg kg^{-1}) were injected from the tail vein. After 60 min of treatment, the inferior vena cava thrombus with blood vessels was separated from rats and used for UCL imaging and ICP-OES measurement. Besides, UCATS-UK (5 mg kg^{-1}) was injected from the tail vein and the inferior vena cava thrombus was separated at setting time points for ICP-OES measurement.

2.22. Pharmacokinetics assay of UK

The male SD rats were divided randomly into 2 groups: UK group and UCATS-UK group (n = 3 for each group). UCATS-UK (5 mg kg^{-1}) and UK (equivalent dose of the loaded UK in UCTAS-UK) were injected into each group from tail vein. Then 1 mL blood was collected from rats at setting time points. The obtained blood was centrifugated at 3000 rpm for 10 min to collect the serum and the concentration of UK was detected by UK Elisa Kit.

2.23. Retention rate and metabolism assay of UCATS-UK in vivo

The male SD rats were injected with UCATS-UK (5 mg kg^{-1}). Then, 200 μL of blood was taken from rats at setting time points and the concentration of silicon was measured by ICP-MS. Besides, after 3 h of injection, the major organs of rats were separated from rats and used for UCL imaging.

2.24. In vivo thrombolysis evaluation

The male SD rats (4 weeks old) were divided randomly into 5 groups: Saline group, NIR group, UK group, UCATS-UK group and UCATS-UK + NIR group (n = 3 for each group). After anaesthesia with isoflurane (3% for inducing and 1% for maintaining anaesthesia) by animal anaesthesia machine (ZS-MV-I), the left femoral veins of the rats were exposed. The filter paper of 3 mm × 5 mm was saturated in 10% $FeCl_3$ and covered on the femoral vein for 3 min. Then, saline, UCATS-UK (5 mg kg^{-1}) and UK (equivalent amount of the loaded UK in UCTAS-UK) were injected from the tail vein. After 60 min, the groups requiring NIR irradiation were irradiated with 2 W cm^{-2} 808 nm NIR for 20 min. After 24 h, the femoral veins were separated for histological analysis.

2.25. In vivo anticoagulation evaluation

Briefly, 4 weeks old male rats were randomly divided into 5 groups: Saline group, NIR group, UK group, UCATS-UK group and UCATS-UK + NIR group (n = 3 for each group). Then, saline, UCATS (5 mg kg^{-1}) and UK (equivalent amount of the loaded UK in UCTAS-UK) were injected from the tail vein, respectively. The filter paper of 2 mm × 4 mm was saturated with 10% $FeCl_3$ and was covered on the carotid artery. Among them, the NIR group and UCATS + NIR group was irradiated with 2 W cm^{-2} 808 nm NIR while filter paper covered on the carotid artery. The carotid artery images before and after thrombosis were recorded by ultrasound imaging (VINNO 6). After that, 2 mL blood of rats in each group was collected for coagulation factors detection by coagulation factor Ⅶ (F Ⅶ) and coagulation factor Ⅸ (F Ⅸ) Elisa Kit. Then, the carotid arteries were separated for histological analysis.

2.26. Statistical analysis

All data obtained were expressed as means ± standard deviation (s.d.). Statistical analyses were performed using GraphPad Prism (GraphPad Software, Inc., San Diego, CA) by the Kolmogorov-Smirnov method to test the normality followed by the one-way analysis of variance (ANOVA) and *t*-test. The threshold of statistical significance was $p < 0.05$.

3. Result and discussion

3.1. Preparation and characterization of UCATS

The multifunctional nanoplatform with targeting thrombolytic and anticoagulative capabilities based on UCNPs was prepared and characterized (Fig. 1A). Since the attenuation of 808 nm NIR in biological tissue is weaker than that of 980 nm NIR [48]. Therefore, the usage of 808 nm NIR could achieve better penetration than 980 nm NIR, as well as avoiding the overheating problem caused by 980 nm NIR [49]. On this basis, we synthesized 808 nm NIR responsive UCNPs [50]. First of all, core@shell@shell nanostructure ($NaYF_4$:Yb,Tm@$NaYF_4$:Nd@$NaYF_4$) that could be excited by 808 nm NIR was synthesized by thermal decomposition method (Fig. 1B). To enable the UCNPs to harvest the 808 nm NIR, a shell layer containing Nd^{3+} ($NaYF_4$:Nd) was coated on the core of $NaYF_4$:Yb,Tm, and the upconversion luminescence (UCL) was further enhanced by coating the outermost layer with an inert $NaYF_4$, which avoided the loss of excitation energy in the nanocrystals. Due to the highly efficient energy transfer from Nd^{3+} to Yb^{3+}, the Nd^{3+} in active shell could absorb the energy of NIR and transfer to Yb^{3+} when UCNPs upon 808 nm NIR excitation. Consequently, the Yb^{3+} ions transferred the energy to the Tm^{3+} ions, thus the UV emissions (340 nm/$^3P_6 - {}^3F_4$ and 360 nm/$^1D_2 - {}^3H_6$) and blue emissions (450 nm/$^1D_2 - {}^3F_4$ and 470 nm/$^1G_4 - {}^3H_6$) of Tm^{3+} could be observed (Figure S1) [33]. The particle sizes of the synthesized hexagonal-phase core, core@shell and core@shell@shell UCNPs were approximately 26 nm, 30 nm and 34 nm, respectively (Figure S2A-C and S3A-C). Subsequently, core@shell@shell UCNPs were coated with mesoporous silica to form the UCM (Fig. 1C) with a particle size of about 70 nm. After that, UCA was obtained by installing the photomechanical azo inside the mesopores, thus achieving the NIR regulated light-controlled drug release. Finally, the platelet targeting molecule tirofiban and SNAP were linked on the outer surface of UCA to obtain the multifunctional nanoplatform UCATS with thrombus-targeting and anticoagulation properties. The transmission electron microscope (TEM) images showed that the UCATS was uniformly distributed, and a 4 nm thin layer on the surface of UCATS could be observed compared with UCM (Fig. 1D), which was consistent with

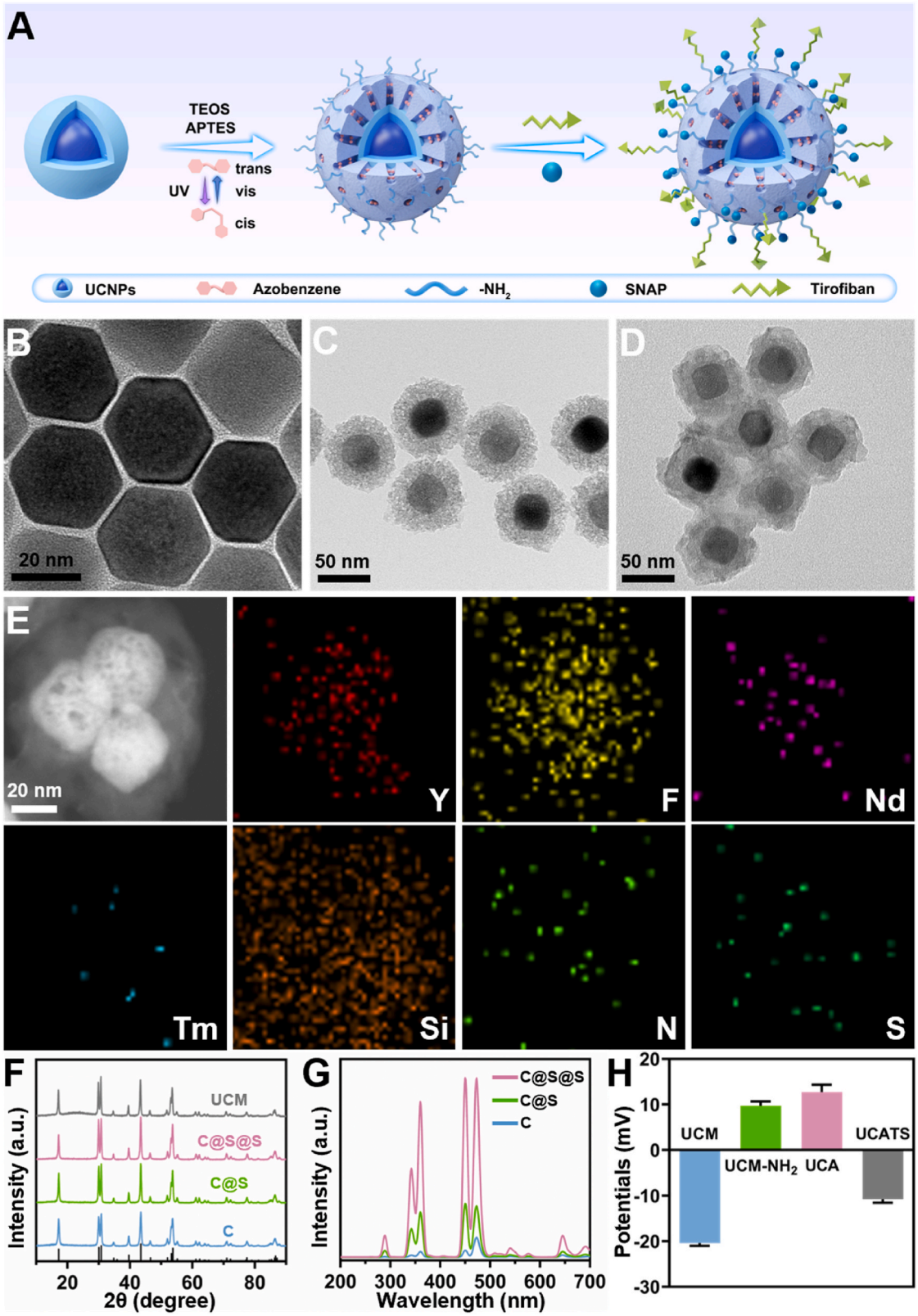

Fig. 1. Synthesis and characteristics of UCATS nanoparticles. A) Synthesis scheme of UCATS. B-D) TEM images of $NaYF_4$:Yb,Tm/$NaYF_4$:Nd/$NaYF_4$, UCM and UCATS, respectively (from left to right). E) Elemental mapping images corresponding to HAADF-STEM image of UCATS. F) XRD patterns of UCM, $NaYF_4$:Yb,Tm/$NaYF_4$:Nd/$NaYF_4$ (C@S@S), $NaYF_4$:Yb,Tm@$NaYF_4$:Nd (C@S), $NaYF_4$:Yb,Tm (C) and the standard data of hexagonal β-$NaYF_4$ (JCPDS No. 016-0334, from top to bottom). G) UCL spectra of $NaYF_4$:Yb,Tm/$NaYF_4$:Nd/$NaYF_4$, $NaYF_4$:Yb,Tm@$NaYF_4$:Nd, $NaYF_4$:Yb,Tm. H) Zeta potentials of UCM, UCM-NH_2, UCA and UCATS. Data are means ± s.d. (n = 3).

the dynamic light scattering (DLS) results (Figure S3E), indicating the successful conjugation of tirofiban and SNAP. Elemental mappings and energy dispersive spectroscopy (EDS) analysis also implied the successful preparation of UCATS (Fig. 1E and S4). The X-ray diffraction (XRD) patterns of UCNPs and UCM were shown in Fig. 1F. All the diffraction peaks could be ascribed to pure hexagonal phase known from β-$NaYF_4$ (JCPDS No. 016-0334). And the broad peak at $2\theta = 22^{\circ}$ of amorphous SiO_2 from mesoporous silica nanoparticles (MSN) could be observed [51]. Besides, the UCL spectra of UCNPs and UCM were explored (Fig. 1G, S5 and S6). After coating the Nd^{3+} shell and inert $NaYF_4$ shell, the UCL intensity of UCNPs appeared greatly enhanced, which could facilitate the drug and NO release from the nanoplatform.

As shown in Fig. 1H, the modification of the amino group on the outer surface of UCM caused the zeta potential to change from negative revers to positive, demonstrating the successful modification of the amino group, which was in accordance with the results of the ninhydrin

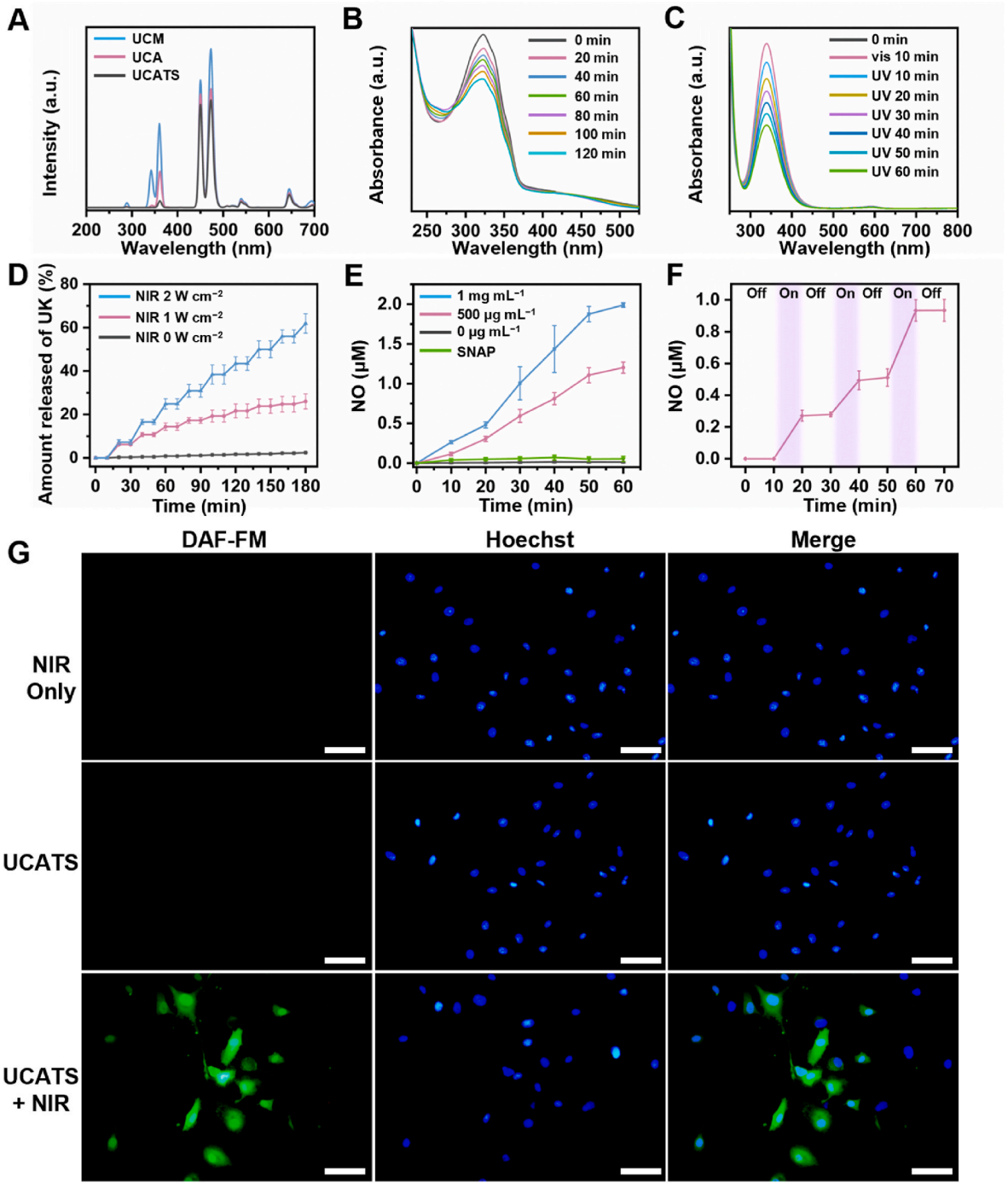

Fig. 2. NIR responsive characteristics of UCATS. A) UCL spectra of UCM, UCA and UCATS. B) UV–vis absorption spectra changes of UCA before and after irradiation with 808 nm NIR light (2 W cm^{-2}). C) UV–vis absorption spectra changes of SNAP before and after irradiation by vis (room light) and UV (365 nm) light for different time. D) NIR-triggered controllable release of UK from UCATS-UK. E) NIR-triggered NO release from UCATS at different concentrations and SNAP. 808 nm NIR: 2 W cm^{-2}. F) On/Off behavior of NO release triggered by 808 nm NIR light (2 W cm^{-2}). G) The fluorescent images of HUVECs stained with NO fluorescent probe (DAF-FM DA) and Hoechst 33342 after being treated with UCATS under dark conditions or 808 nm NIR irradiation (1 W cm^{-2}). Scale bar = 50 μm. Data are means ± s.d. (n = 3).

reaction (Figure S7). The potential of UCA was slightly increased compared with UCNP@mSiO$_2$-NH$_2$ (UCM-NH$_2$), indicating that azo was modified in the pores of mesoporous silica (MSN), and finally the connection of tirofiban and SNAP changed the potential of UCATS from positive to negative. Fourier transform infrared (FT-IR) results showed that the characteristic frequency at 1385 cm^{-1} could be assigned to C−N stretching vibration of azo, and the characteristic peaks of the amide group appeared at 1460 cm^{-1}, 1553 cm^{-1} and 1645 cm^{-1} indicated the successful modification of tirofiban and SNAP (Figure S8). Meanwhile, the result of UV–vis absorption spectra also demonstrated the synthesis of UCATS (Figure S9). Also, we analyzed the modification rate of SNAP and tirofiban. While the molar ratio of SNAP and tirofiban was at 1:1, the SNAP and tirofiban achieved the most optimal modification rate of about 5.2% and 4.3%, respectively (Figure S10). In addition, the thermogravimetric (TG) analysis determined of about 7.0 wt% of modified azobenzene in the mesopores, which reduced the specific surface area and pore size of the UCM from 537 cm^3 g^{-1} and 12.2 nm to 263 cm^3 g^{-1} and 11.4 nm, (Figure S11), resulting in a final UK loading content of about 6.4 wt% (Figure S12).

3.2. Assessment of NIR-Triggered UK and NO release

To further testify the properties of nanoplatform for controlled release of drugs and NO, we firstly verified whether azo and SNAP could absorb UCL. From the UV–vis absorption spectra and UCL spectra (Figure S13 and S14), it could be found that the absorption spectra of azo and SNAP partially overlapped with the UCL, which indicated that azo and SNAP could effectively absorb the energy of UV/blue light emitted by UCNPs. As manifested in Fig. 2A, compared with UCM, the UCL of UCA was significantly decreased in both UV and blue light, especially in the UV light. After being modified with SNAP, UV light was almost completely absorbed, demonstrating that azo and SNAP could efficiently absorb the energy of UCL, which is beneficial to release drug or NO. Interestingly, the absorption of UV/blue light by azo and SNAP could also reduce the damage to biological tissues in a considerable extent. UV–vis absorption spectra of UCA before and after NIR light irradiation with different time intervals were also shown in Fig. 2B, which further proved that azo only responded to UCL (Figure S15). In addition, as illustrated in Fig. 2C, SNAP only responded to UV light and could hardly absorb visible light and NIR, as well as had no significant degradation in phosphate buffer saline (PBS) solution, which indicated that SNAP was stable (Figure S16). Besides, the UCATS was also stable in saline or PBS solution within 14 d (Figure S17).

To evaluate the property of the NIR-triggered release of UK, UCATS-UK was exposed under different power densities of 808 nm NIR irradiation. By monitoring the released amount of UK from the nanoplatform under intermittent NIR irradiation conditions, it was suggested that the UK release was dependent on the power density and irradiation time of NIR (Fig. 2D). After 3 h, the release amount of UK reached about 26% under intermittent NIR irradiation at 1 W cm^{-2}, and maximum release amount of about 62% at 2 W cm^{-2}. While in the absence of NIR, the released UK was barely detectable. These results proved that a precise control of UK release from the nanoplatform could be achieved through adjusting the NIR exposure time and power density.

Subsequently, we assessed the NO release capacity of UCATS under 808 nm NIR irradiation (Figure S18). The results suggested that the released concentration of NO was positively correlated with the concentration of UCATS (Fig. 2E). Also, we investigated the effect of power density of 808 nm NIR on NO release from UCATS. The result showed that the NO release rate decreased with the reduction of the power density of 808 nm NIR (Figure S19). In addition, on-demand and light-controlled NO release was also investigated. As illustrated in Fig. 2F, NO was released only under the NIR irradiation, indicating that UCATS had excellent NIR controllability of NO release. It has been reported in the literatures that the biological effects of NO may be altered in a concentration-dependent manner [52]. For example, NO inhibits platelet function at higher concentrations, while at lower concentrations it may activate platelet function. As a highly reactive chemical, NO has a short diffusion radius (40–200 μm) [53]. Therefore, delivery of NO to platelets in a light-triggered and targeted manner would be more effective and desirable [54]. For investigating the *in vivo* release capacity of NO, we designed intracellular NIR-triggered NO release experiments. The fluorescent probe 4-amino-5-methylamino-2,7-difluorofluorescein diacetate (DAF-FM DA) was incubated with the human umbilical vein endothelial cells (HUVECs) to detect NO release. Although DAF-FM DA initially had a very low fluorescence, it could react with NO and exhibit an extremely strong green fluorescence. As shown in Fig. 2G, the green fluorescence was detected in HUVECs only when both UCATS and NIR irradiation were present (Figure S20). The results indicated that we could effectively control the on-demand NO release from UCATS *in vivo* by NIR irradiation.

3.3. Evaluation of thrombolysis, anticoagulative and targeting ability in vitro

After verifying the light-controlled release properties of the nanoplatform, we further evaluated the thrombolytic and anticoagulative capacities of the nanoplatform *in vitro*. First, we designed a static thrombolysis assay to evaluate the *in vitro* thrombolytic capacity of UCATS-UK (Fig. 3A). As manifested in Fig. 3B, after 6 h treatment (2 W cm^{-2} NIR irradiation for 10 min per hour), significant thrombolysis occurred in the UK, UCA-UK + NIR and UCATS-UK + NIR groups, indicating that only under NIR irradiation, UCA-UK and UCATS-UK could release UK to dissolve the thrombus (Fig. 3C and S21). Meanwhile, no significant thrombolysis was observed in NIR group, suggesting that thrombolysis in UCA-UK + NIR and UCATS-UK + NIR groups was contributed to the NIR-triggered UK release. Besides, the UCATS-UK + NIR group (0%) exhibited more significant thrombolytic effect than that of UK group (approximately 31.53%) due to the targeted aggregation of UCATS-UK on the thrombus site, which promoted the utilization of UK and enhanced thrombolysis. Also, we detected the OD_{415} of the supernatant in each group as indicator of fibrin (Figure S22), which was consistent with the result of Fig. 3B.

To validate the thrombolytic ability of nanoplatform in the simulated vasculature, we constructed a dynamic thrombotic model comprised a constant flow pump and a simulated 3D printed vein vasculature to imitate *in vivo* thrombolysis (Fig. 3D and E). The 3D printed vein vasculature was used to fix and block the thrombus, while the simulated circulating blood flow was propelled with constant flow pump. The simulated blood flow circulation facilitated the enrichment of thrombolytic drugs and nanoplatform at the thrombus site and accelerated thrombolysis. According to the results, although shear forces of circulating simulated blood on the thrombus resulted in partial dissolution of the thrombus, UCA-UK and UCATS-UK still required NIR irradiation to achieve more effective thrombolysis (Fig. 3F), which was consistent with the trend in static thrombolysis results.

NO can promote intracellular cyclic guanosine monophosphate (cGMP) synthesis and decrease the intracytoplasmic Ca^{2+} concentration of platelets, thereby inhibiting platelet activation and aggregation [52,55,56]. Theoretically, as long as the activation and aggregation of platelets can be inhibited, the formation of thrombus can be prevented. Consequently, we performed platelet aggregation experiment to validate the anticoagulative capability of the nanoplatform *in vitro* [57]. As shown in Fig. 3G, in the Saline group, most platelets (approximately 70.6%) aggregated rapidly in response to the stimulation of platelet activator adenosine diphosphate (ADP). At the same time, the NIR group showed comparable result (approximately 64.3%), suggesting that NIR had no inhibitory effect on ADP-induced platelet aggregation. Also, equivalent amount of modified tirofiban was not sufficient to inhibit most platelet aggregation (approximately 55.8%). Furthermore, The SNAP + NIR group slightly reduced platelet aggregation (approximately 41.6%), which might be attributed to the small amount released NO

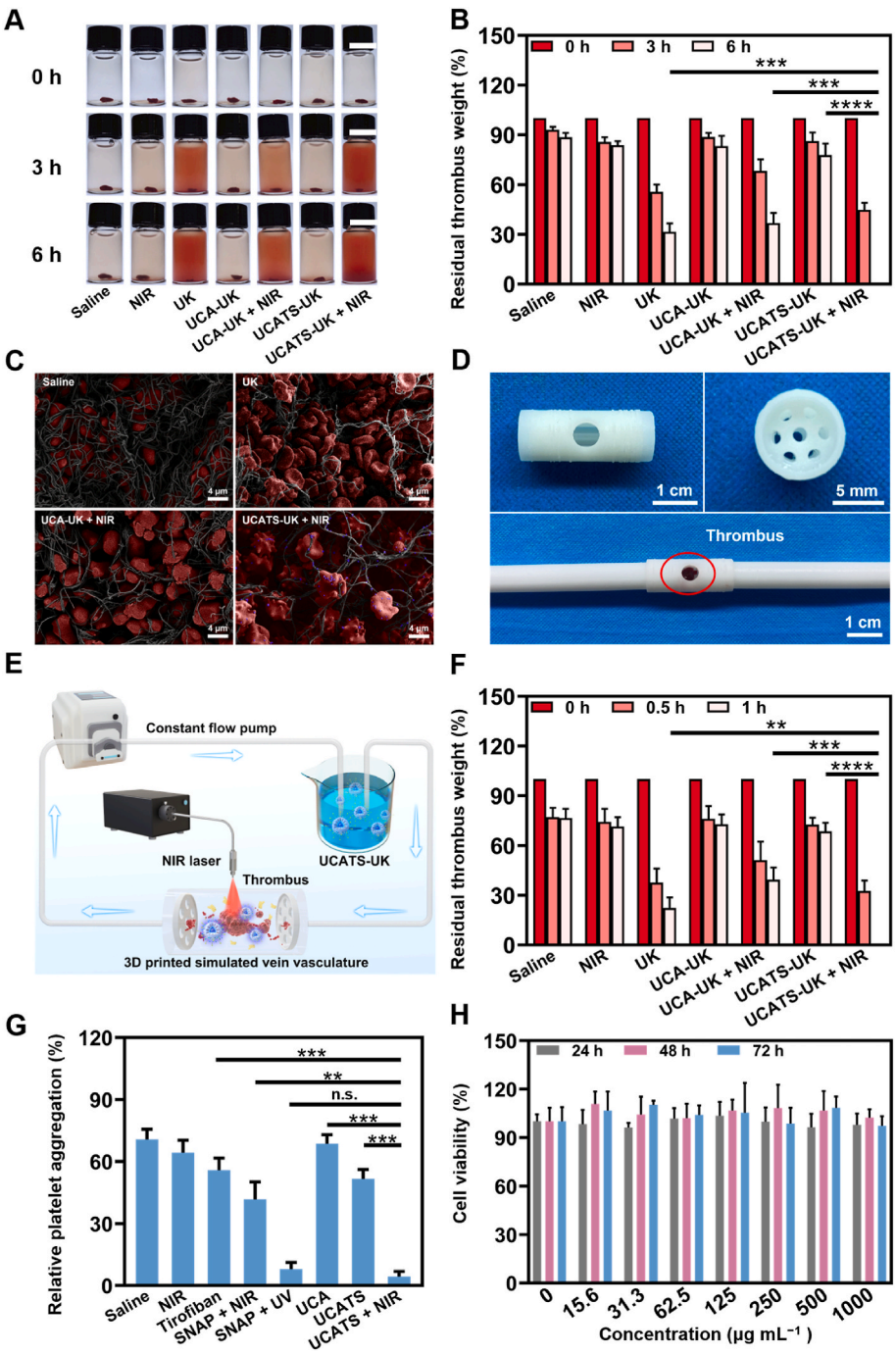

Fig. 3. *In vitro* thrombolysis and anticoagulation of UCATS-UK. A) Static thrombolysis and B) residual thrombus weight in static thrombolysis. C) Representative SEM images of thrombus in static thrombolysis model after treatment with saline, UK, UCA-UK + NIR and UCATS-UK + NIR for 3 h. (The fibrin was grey, red blood cells were red and UCATS-UK was blue). D) The photographs of 3D printed vein vasculature. E) Schematic illustration of dynamic thrombolysis model and F) residual thrombus weight in dynamic thrombolysis. G) Analysis of inhibiting platelet aggregation after different treatments. H) Cell viability of UCATS-UK at different concentrations to HUVECs at 24 h, 48 h and 72 h, respectively. Scale bar = 1 cm. Data are means ± s.d. (n = 3). $^{*}p < 0.05$, $^{**}p < 0.01$, $^{***}p < 0.001$, $^{****}p < 0.0001$.

from SNAP caused by the increased temperature after long-term NIR irradiation. In addition, the UCA could hardly inhibit platelet aggregation (approximately 68.6%). The reduction of platelet aggregation in the UCATS group (approximately 52.3%) might be due to the surface-modified tirofiban that could partly inhibit the activation and aggregation of platelets. However, the SNAP + UV group showed slight aggregation of platelets (approximately 7.8%), which was almost equivalent to that of the UCATS + NIR group (approximately 4.3%). Compared with native UCATS group, NO produced under NIR irradiation in UCATS + NIR group significantly inhibited platelets activation and aggregation, which indicated that the capability of UCATS inhibiting platelet aggregation was mainly attributed to the NO released from UCATS under NIR irradiation. Besides, to ensure that UCATS could only target to the activated platelets, we carried out platelet targeting assay [47]. After co-culture of activated and non-activated platelets with UCATS, the content of Nd^{3+} in non-activated platelets group could hardly be detected. However, a significant higher content of Nd^{3+} was detected in activated platelets group, which indicated that UCATS could specifically target to the activated platelets and would not target to non-activated platelets in circulation system (Figure S23).

3.4. Cytotoxicity assessment in vitro

An ideal drug delivery nanoplatform should have reliable biocompatibility. On this account, the cytotoxicity experiments and Live/Dead cell staining experiments using HUVECs and mouse fibroblast cells (L929) were performed to prove the biosafety of UCATS-UK. All the results demonstrated that the nanoplatform possessed excellent

biosafety (Fig. 3H and S24-S26). Also, the UV emitted from UCATS would damage biological tissues was evaluated. As shown in Figure S27, after co-culture with UCATS and under 808 nm NIR irradiation, the cell viability of HUVECs was still over 80%, proving that UCATS combined with NIR could be safely used as well. Meanwhile, the results of hemolysis assay showed that the hemolysis rates of UCATS at different concentrations were less than 5%, which suggested that UCATS had good biocompatibility (Figure S28).

3.5. Cytotoxicity assessment in vitro and evaluation of laser safety

Besides, the photothermal effect of NIR should be considered for *in vitro* and *in vivo* applications. Therefore, we tested the temperature changes *in vitro* and *in vivo* under 808 nm and 980 nm NIR irradiation. It could be found that the temperature of PBS increased by only 0.6 °C under 2 W cm^{-2} 808 nm NIR irradiation for 10 min, while the temperature of the 980 nm irradiation group increased by 22.3 °C within 10 min (Figure S29A). For animal experiments, although the skin temperature increased by 2.4 °C after 10 min of 2 W cm^{-2} 808 nm NIR irradiation, it was still within the safe range, while the skin temperature of rat increased by nearly 10 °C during 3 min of 2 W cm^{-2} 980 nm NIR irradiation (Figure S29B), which suggested that 808 nm NIR could be safely used *in vitro* and *in vivo*. Moreover, the Live/Dead cell staining also confirmed the good biosafety of 808 nm NIR light (Figure S30).

3.6. Evaluation of thrombus targeting and thrombolysis abilities in vivo

Inspired by the desirable thrombolytic and anticoagulant capacities of UCATS-UK *in vitro*, we further tested its feasibility for application *in vivo*. Firstly, the rat inferior vena cava thrombus model was established to verify the thrombus targeting ability of UCATS *in vivo*. Limited by the penetration and intensity of UCL, we separated the inferior vena cava thrombus with blood vessels from rats and used them for UCL imaging (Figure S31). As shown in Fig. 4A, no significant fluorescence was

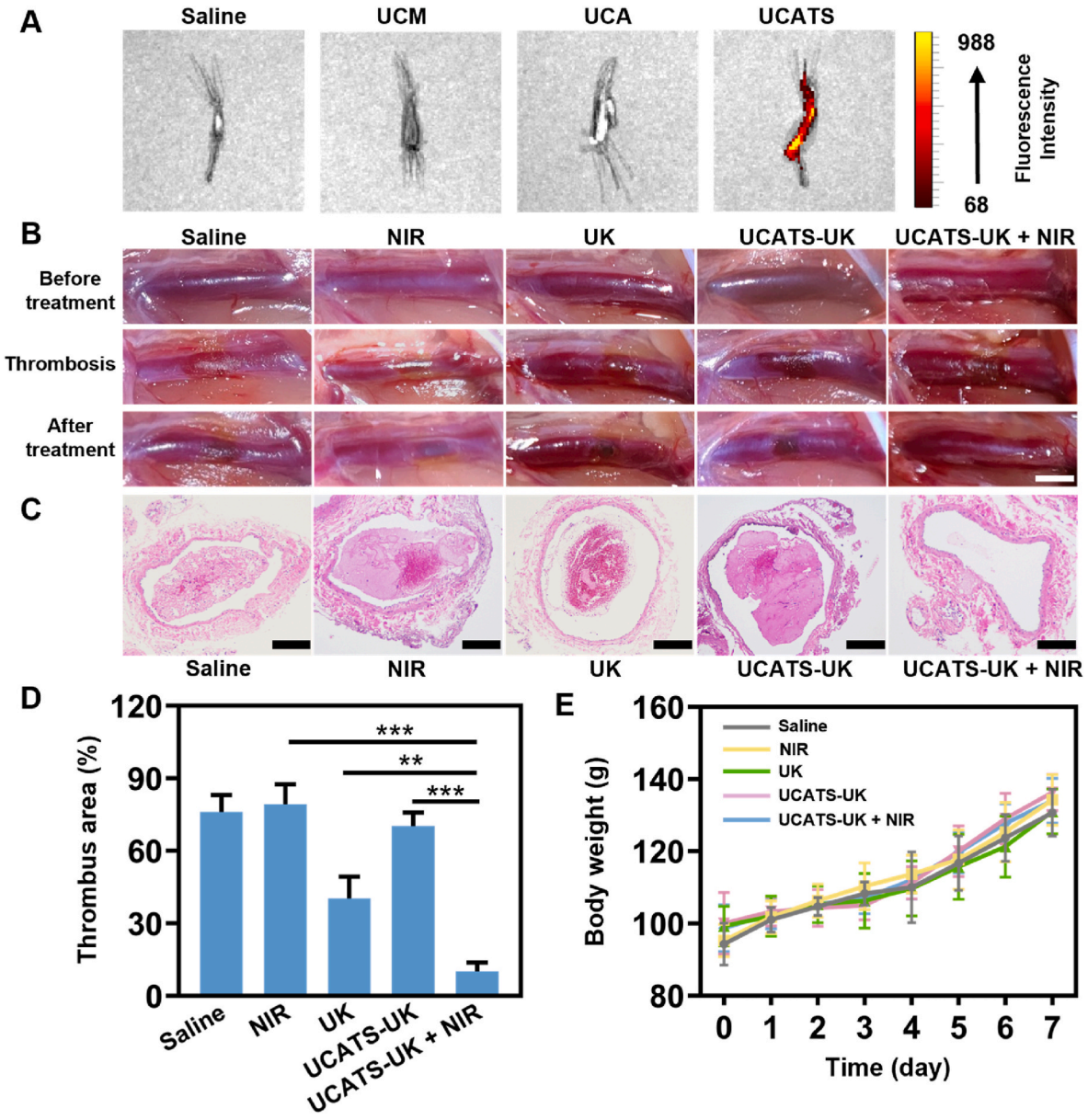

Fig. 4. *In vivo* targeting and thrombolytic effects of UCATS-UK. A) The fluorescence images of inferior vena cava (IVC) thrombus from rats after being treated with different samples. B) The photographs of femoral vein at different conditions in each group. Scale bar = 2 mm. C) H&E staining images of each group. Scale bar = 200 μm. D) Quantification of the thrombus area in femoral vein in each group. E) The body weight of rats in each group. Data are means ± s.d. (n = 3). $^{*}p < 0.05$, $^{**}p < 0.01$, $^{***}p < 0.001$.

detected in the Saline, UCM or UCA groups. On the contrary, a visible UCL signal was detected in the UCATS group, indicating that the modification of tirofiban could endow the nanoplatform with thrombus targeting property. In addition, we isolated the thrombus from the inferior vena cava and assayed the Nd^{3+} content of the thrombus, the results suggested that UCATS had successfully accumulated on the thrombus site (Figure S32), which was consistent with UCL imaging results *in vivo*. Besides, we also tested when UCATS-UK reached maximum enrichment at the thrombus site, which could be used for guiding the treatment of light-controlled drug release. As shown in Figure S33, the maximum enrichment of UCATS at the thrombus site was at the time of 60 min after injection, which was the best time for NIR irradiation treatment. In short, the favorable targeting ability of UCATS was conducive to the treatment of thrombus *in vivo*, improved the bioavailability of the thrombolytic drug, and reduced the side effects caused by overdose [58].

Then, the drug pharmacokinetics of native UK and UCATS-UK in rats was studied. As manifested in Figure S34, the half-life of native UK in rats was about 16 min. While under NIR irradiation, the concentration of UK increased gradually in UCATS-UK group and the half-life of UK was prolonged to nearly 110 min, which was beneficial to enhance the bioavailability of UK. Besides, the retention rate and metabolism of UCATS-UK in rats were also investigated. It could be found in Figure S35 that nearly half of the nanomaterials still remained in the rats after 2 h of injection, which was beneficial for the application of UCATS-UK *in vivo*. Furthermore, the UCL imaging showed that the kidney had the highest fluorescence intensity, which indicated that the UCATS-UK was mainly metabolized by kidney.

Afterward, rat femoral vein thrombus models were constructed to assess the thrombolytic capacity of the nanoplatform *in vivo*. Photographs of femoral vein thrombosis before and after treatment in each group (Fig. 4B) showed that UCATS-UK exhibited significant thrombolytic effect under NIR irradiation, with almost no intravascular thrombus (black areas). By contrast, although UCATS-UK prolonged the *in vivo* half-life of UK and targeted delivery to the thrombus site, the consistently black areas in the UCATS-UK group illustrated that UCATS-UK could not exhibit significant thrombolytic capacity due to the inhibition of UK release without NIR irradiation. In other words, UCATS-UK could be safely applied for *in vivo* thrombolysis by NIR-controlled release of UK. Owing to the rapid metabolism of UK *in vivo*, the native UK group exhibited only partial thrombus dissolution. In addition, we analyzed the femoral vein thrombus after treating with each group by hematoxylin and eosin (H&E) staining (Fig. 4C), which was almost identical to the results observed in Fig. 4B. Quantitative analysis of residual thrombus in vascular cross-sectional area for H&E staining in Fig. 4D also manifested that UCATS-UK + NIR group had the best thrombolytic effect (approximately 10.1%). Besides, the rats in each group showed no significant differences in body weight, meaning that the nanoplatform did not affect the growth of rats (Fig. 4E). Also, no obvious inflammation or injury appeared in H&E staining of major organs (Figure S36), demonstrating that the nanoplatform owned excellent biocompatibility.

3.7. Evaluation of anticoagulability in vivo

Due to the high recurrence risk of thrombus after revascularization, the anticoagulative therapy after thrombolysis is equally essential. To evaluate that NIR-triggered NO release from UCATS possessed antithrombotic activity, rat carotid arterial thrombus models were used in this work (Figure S37). Since intravascular thrombosis could not be directly observed, the ultrasound imaging was used to monitor the carotid artery thrombosis in real time. As manifested in Fig. 5A, thrombotic signal could hardly be detected in the carotid arterial of the UCATS + NIR group, demonstrating that UCATS was able to release NO under NIR irradiation to inhibit platelet activation and thus prevented thrombus formation. As shown in Fig. 5B and C, the H&E staining of carotid arterial thrombus and quantitative analysis results were also validated that UCATS + NIR group exhibited the best antithrombotic capability (approximately 16.0%) compared with the Saline, NIR, UK and UCATS groups (approximately 89.3%, 87.8%, 85.7%, and 75.3%, respectively). After treatment, the coagulation functions of rats in UCATS + NIR group showed no significant difference compared with Saline group, meaning that NO was an effective anticoagulant and avoid the bleeding risk (Figure S38). The above results demonstrated that the nanoplatform

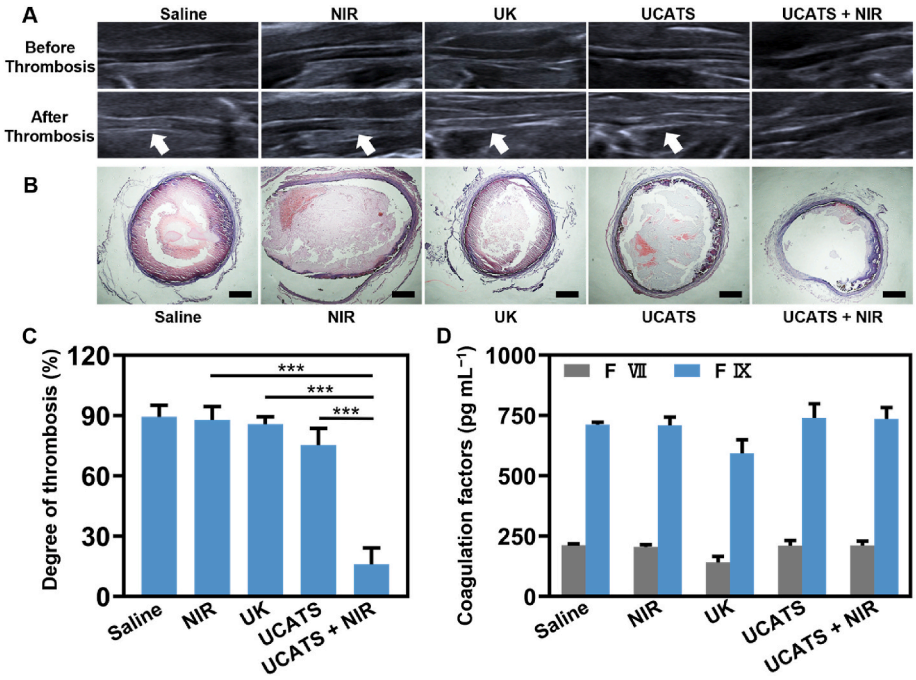

Fig. 5. *In vivo* anticoagulative effect of UCATS. A) Ultrasound images of carotid artery in rats before and after thrombosis in each group (white arrows indicate thrombus). B) H&E staining images of each group. Scale bar = 200 μm. C) Quantitative analysis of the thrombosis degree in each group. D) The coagulation factors of rats after different treatments. Data are means ± s.d. (n = 3). $^{*}p < 0.05$, $^{**}p < 0.01$, $^{***}p < 0.001$.

could not only enable targeted thrombolysis, but also act as a non-pharmacological anticoagulant to prevent the recurrence of thrombus. Although the UCATS exerted excellent anticoagulative effect under NIR irradiation, whether UCATS would affect coagulation factors should also be investigated. Since the coagulation factor Ⅶ (F Ⅶ) and coagulation factor Ⅸ (F Ⅸ) exert coagulation functions through the extrinsic and intrinsic coagulation pathways respectively, the contents of F Ⅶ and F Ⅸ can reflect the functional status of extrinsic and intrinsic coagulation [59]. As manifested in Fig. 5D and S39, either UCATS group or UCATS + NIR group showed no influence on the F Ⅶ and F Ⅸ, which demonstrated that UCATS could be safely applied *in vivo*.

4. Conclusion

In summary, we developed an upconversion nanoparticle-based targeted thrombolytic and anticoagulation nanoplatform. The nanoplatform could realize light-controlled UK and NO release under NIR irradiation. Compared with the conventional treatment strategy of UK combined with heparin, the nanoplatform could achieve thrombolytic and anticoagulation therapy simultaneously with minimizing drug induced bleeding risk. Also, if the release of UK and NO could be controlled separately, the long-term anticoagulation effect followed by thrombolysis therapy could be realized. Additionally, the introduction of UCNPs realized the possibility of thrombus imaging. However, limitations in UCL intensity and penetration depth prevented the application of *in vivo* thrombus imaging. If the intensity and penetration of UCL can be enhanced (e.g., NIR-II UCL emission), it will be expected to construct an integrated nanoplatform for imaging, diagnosis and treatment of thrombus in the future.

CRediT authorship contribution statement

Shichen Liu: Conceptualization, Methodology, Software, Writing – original draft. **Yao Sun:** Data curation, Methodology. **Teng Zhang:** Investigation, Methodology. **Longtao Cao:** Formal analysis, Data curation. **Zhiwei Zhong:** Visualization, Software. **Haoxin Cheng:** Validation. **Qingqing Wang:** Methodology, Software. **Zhuang Qiu:** Methodology. **Weimin Zhou:** Supervision, Funding acquisition. **Xiaolei Wang:** Validation, Project administration, Writing – review & editing, Funding acquisition.

Declaration of competing interest

All authors declared that no conflict interest existed.

Acknowledgements

This work was funded by the National Natural Science Foundation of China (No. 31860263 to Xiaolei Wang; No. 82060095 to Weimin Zhou), Key Youth Project of Jiangxi Province (20202ACB216002 to Xiaolei Wang), Natural Science Foundation of Jiangxi Province (911135755018 to Weimin Zhou) and Jiangxi Provincial Graduate Innovation Special Fund (YC2020-B053 to Shichen Liu).

Appendix A. Supplementary data

Supplementary data to this article can be found online at https://doi.org/10.1016/j.bioactmat.2022.03.013.

References

[1] F. Khan, T. Tritschler, S.R. Kahn, M.A. Rodger, Venous thromboembolism, Lancet 398 (2021) 64–77.
[2] S.Z. Goldhaber, H. Bounameaux, Pulmonary embolism and deep vein thrombosis, Lancet 379 (2012) 1835–1846.
[3] E. Renner, G.D. Barnes, Antithrombotic management of venous thromboembolism: JACC focus seminar, J. Am. Coll. Cardiol. 76 (2020) 2142–2154.
[4] M.J. Stubbs, M. Mouyis, M. Thomas, Deep vein thrombosis, BMJ 360 (2018) k351.
[5] R.H. Strijkers, A.J. Cate-Hoek, S.F. Bukkems, C.H. Wittens, Management of deep vein thrombosis and prevention of post-thrombotic syndrome, BMJ 343 (2011), d5916.
[6] N. Mackman, Triggers, targets and treatments for thrombosis, Nature 451 (2008) 914–918.
[7] N. Mackman, W. Bergmeier, G.A. Stouffer, J.I. Weitz, Therapeutic strategies for thrombosis: new targets and approaches, Nat. Rev. Drug Discov. 19 (2020) 333–352.
[8] B. Engelmann, S. Massberg, Thrombosis as an intravascular effector of innate immunity, Nat. Rev. Immunol. 13 (2013) 34–45.
[9] T. Sumii, E.H. Lo, Involvement of matrix metalloproteinase in thrombolysis-associated hemorrhagic transformation after embolic focal ischemia in rats, Stroke 33 (2002) 831–836.
[10] E.-P. Investigators, H.R. Buller, M.H. Prins, A.W. Lensin, H. Decousus, B. F. Jacobson, E. Minar, J. Chlumsky, P. Verhamme, P. Wells, G. Agnelli, A. Cohen, S. D. Berkowitz, H. Bounameaux, B.L. Davidson, F. Misselwitz, A.S. Gallus, G. E. Raskob, S. Schellong, A. Segers, Oral rivaroxaban for the treatment of symptomatic pulmonary embolism, N. Engl. J. Med. 366 (2012) 1287–1297.
[11] S. Middeldorp, M.H. Prins, B.A. Hutten, Duration of treatment with vitamin K antagonists in symptomatic venous thromboembolism, Cochrane Database Syst. Rev. 8 (2014), CD001367.
[12] N. Chan, M. Sobieraj-Teague, J.W. Eikelboom, Direct oral anticoagulants: evidence and unresolved issues, Lancet 396 (2020) 1767–1776.
[13] A.L. Papa, A. Jiang, N. Korin, M.B. Chen, E.T. Langan, A. Waterhouse, E. Nash, J. Caroff, A. Graveline, A. Vernet, A. Mammoto, T. Mammoto, A. Jain, R.D. Kamm, M.J. Gounis, D.E. Ingber, Platelet decoys inhibit thrombosis and prevent metastatic tumor formation in preclinical models, Sci. Transl. Med. 11 (2019), eaau5898.
[14] Y. Zhang, J. Yu, J. Wang, N.J. Hanne, Z. Cui, C. Qian, C. Wang, H. Xin, J.H. Cole, C. M. Gallippi, Y. Zhu, Z. Gu, Thrombin-responsive transcutaneous patch for auto-anticoagulant regulation, Adv. Mater. 29 (2017), 1604043.
[15] H. Zhu, X.J. Loh, E. Ye, Z. Li, Polymeric matrix-based nanoplatforms toward tumor therapy and diagnosis, ACS Mater. Lett. 4 (2021) 21–48.
[16] H.W. Cheng, X.S. Fan, E.Y. Ye, H. Chen, J. Yang, L.J. Ke, M.L. You, M.T. Liu, Y. W. Zhang, Y.L. Wu, G. Liu, X.J. Loh, Z.B.A. Li, Dual tumor microenvironment remodeling by glucose-contained radical copolymer for MRI-guided photoimmunotherapy, Adv. Mater. (2021), 2107674.
[17] Z. Luo, Y. Xu, E. Ye, Z. Li, Y.L. Wu, Recent progress in macromolecule-anchored hybrid gold nanomaterials for biomedical applications, Macromol. Rapid Commun. 40 (2019), e1800029.
[18] A. Suwardi, F.K. Wang, K. Xue, M.Y. Han, P.L. Teo, P. Wang, S.J. Wang, Y. Liu, E. Y. Ye, Z.B. Li, X.J. Loh, Machine learning-driven biomaterials evolution, Adv. Mater. 34 (2022), 2102703.
[19] J.C. Xu, Y.L. Zhang, J.Q. Xu, G.N. Liu, C.Z. Di, X. Zhao, X. Li, Y. Li, N.B. Pang, C. Z. Yang, Y.Y. Li, B.Z. Li, Z.F. Lu, M.F. Wang, K.S. Dai, R. Yan, S.P. Li, G.J. Nie, Engineered nanoplatelets for targeted delivery of plasminogen activators to reverse thrombus in multiple mouse thrombosis models, Adv. Mater. 32 (2020), 1905145.
[20] Y. Teng, H. Jin, D. Nan, M. Li, C. Fan, Y. Liu, P. Lv, W. Cui, Y. Sun, H. Hao, X. Qu, Z. Yang, Y. Huang, *In vivo* evaluation of urokinase-loaded hollow nanogels for sonothrombolysis on suture embolization-induced acute ischemic stroke rat model, Bioact. Mater. 3 (2018) 102–109.
[21] Q.Q. Deng, L. Zhang, W. Lv, X.M. Liu, J.S. Ren, X.G. Qu, Biological mediator-propelled nanosweeper for nonpharmaceutical thrombus therapy, ACS Nano 15 (2021) 6604–6613.
[22] M. Wan, Q. Wang, R. Wang, R. Wu, T. Li, D. Fang, Y. Huang, Y. Yu, L. Fang, X. Wang, Y. Zhang, Z. Miao, B. Zhao, F. Wang, C. Mao, Q. Jiang, X. Xu, D. Shi, Platelet-derived porous nanomotor for thrombus therapy, Sci. Adv. 6 (2020), eaaz9014.
[23] X. Tian, T. Fan, W. Zhao, G. Abbas, B. Han, K. Zhang, N. Li, N. Liu, W. Liang, H. Huang, W. Chen, B. Wang, Z. Xie, Recent advances in the development of nanomedicines for the treatment of ischemic stroke, Bioact. Mater. 6 (2021) 2854–2869.
[24] A. Zenych, L. Fournier, C. Chauvierre, Nanomedicine progress in thrombolytic therapy, Biomaterials 258 (2020), 120297.
[25] A. Zenych, C. Jacqmarcq, R. Aid, L. Fournier, L.M. Forero Ramirez, F. Chaubet, T. Bonnard, D. Vivien, D. Letourneur, C. Chauvierre, Fucoidan-functionalized polysaccharide submicroparticles loaded with alteplase for efficient targeted thrombolytic therapy, Biomaterials 277 (2021), 121102.
[26] X.L. Wang, C.C. Wei, M.K. Liu, T. Yang, W.M. Zhou, Y. Liu, K. Hong, S.H. Wang, H. B. Xin, X.W. Ding, Near-infrared triggered release of uPA from nanospheres for localized hyperthermia-enhanced thrombolysis, Adv. Funct. Mater. 27 (2017), 1701824.
[27] L. Lan, Y.J. Sun, X.Y. Jin, L.J. Xie, L. Liu, L. Cheng, A light-controllable chemical modulation of m(6)A RNA methylation, Angew. Chem. Int. Ed. 60 (2021) 18116–18121.
[28] Y. Zhang, Y. Zhang, G. Song, Y. He, X. Zhang, Y. Liu, H. Ju, A DNA-azobenzene nanopump fueled by upconversion luminescence for controllable intracellular drug release, Angew. Chem. Int. Ed. 58 (2019) 18207–18211.
[29] L. Jiang, D. Chen, Z. Jin, C. Xia, Q. Xu, M. Fan, Y. Dai, J. Liu, Y. Li, Q. He, Light-triggered nitric oxide release and structure transformation of peptide for enhanced intratumoral retention and sensitized photodynamic therapy, Bioact. Mater. 12 (2022) 303–313.
[30] B.T. Huy, A.P. Kumar, T.T. Thuy, N.N. Nghia, Y.I. Lee, Recent advances in fluorescent upconversion nanomaterials: novel strategies for enhancing optical and magnetic properties to biochemical sensing and imaging applications, Appl. Spectrosc. Rev. (2020) 1–35.

[31] S. Han, R. Deng, Q. Gu, L. Ni, U. Huynh, J. Zhang, Z. Yi, B. Zhao, H. Tamura, A. Pershin, H. Xu, Z. Huang, S. Ahmad, M. Abdi-Jalebi, A. Sadhanala, M.L. Tang, A. Bakulin, D. Beljonne, X. Liu, A. Rao, Lanthanide-doped inorganic nanoparticles turn molecular triplet excitons bright, Nature 587 (2020) 594–599.
[32] G. Jalani, V. Tam, F. Vetrone, M. Cerruti, Seeing, targeting and delivering with upconverting nanoparticles, J. Am. Chem. Soc. 140 (2018) 10923–10931.
[33] S. Wu, H.J. Butt, Near-infrared-sensitive materials based on upconverting nanoparticles, Adv. Mater. 28 (2016) 1208–1226.
[34] Y. Zhang, X. Zhu, Y. Zhang, Exploring heterostructured upconversion nanoparticles: from rational engineering to diverse applications, ACS Nano 15 (2021) 3709–3735.
[35] C. Sun, M. Gradzielski, Advances in fluorescence sensing enabled by lanthanide-doped upconversion nanophosphors, Adv. Colloid Interface Sci. (2021), 102579.
[36] J. Liu, W. Bu, L. Pan, J. Shi, NIR-triggered anticancer drug delivery by upconverting nanoparticles with integrated azobenzene-modified mesoporous silica, Angew. Chem. Int. Ed. 52 (2013) 4375–4379.
[37] X. Li, L. Zhou, Y. Wei, A.M. El-Toni, F. Zhang, D. Zhao, Anisotropic growth-induced synthesis of dual-compartment Janus mesoporous silica nanoparticles for bimodal triggered drugs delivery, J. Am. Chem. Soc. 136 (2014) 15086–15092.
[38] K. Wang, Q. Wu, X. Wang, G. Liang, A. Yang, J. Li, Near-infrared control and real-time detection of osteogenic differentiation in mesenchymal stem cells by multifunctional upconversion nanoparticles, Nanoscale 12 (2020) 10106–10116.
[39] A. Meyer, J. Auernheimer, A. Modlinger, H. Kessler, Targeting RGD recognizing integrins: drug development, biomaterial research, tumor imaging and targeting, Curr. Pharmaceut. Des. 12 (2006) 2723–2747.
[40] B.D. Adair, J.L. Alonso, J. van Agthoven, V. Hayes, H.S. Ahn, I.S. Yu, S.W. Lin, J. P. Xiong, M. Poncz, M.A. Arnaout, Structure-guided design of pure orthosteric inhibitors of alphaIIbbeta3 that prevent thrombosis but preserve hemostasis, Nat. Commun. 11 (2020) 398.
[41] Y. Zhao, R. Xie, N. Yodsanit, M. Ye, Y. Wang, S. Gong, Biomimetic fibrin-targeted and H_2O_2-responsive nanocarriers for thrombus therapy, Nano Today 35 (2020), 100986.
[42] X. Chen, F. Jia, Y. Li, Y. Deng, Y. Huang, W. Liu, Q. Jin, J. Ji, Nitric oxide-induced stromal depletion for improved nanoparticle penetration in pancreatic cancer treatment, Biomaterials 246 (2020), 119999.
[43] H. Qiu, P. Qi, J. Liu, Y. Yang, X. Tan, Y. Xiao, M.F. Maitz, N. Huang, Z. Yang, Biomimetic engineering endothelium-like coating on cardiovascular stent through heparin and nitric oxide-generating compound synergistic modification strategy, Biomaterials 207 (2019) 10–22.
[44] Y. Zhao, P.M. Vanhoutte, S.W. Leung, Vascular nitric oxide: beyond eNOS, J. Pharmacol. Sci. 129 (2015) 83–94.
[45] R.C. Jin, J. Loscalzo, Vascular nitric oxide: formation and function, Hematol. Res. Rev. 2010 (2010) 147–162.
[46] N.J.J. Johnson, A. Korinek, C. Dong, F.C.J.M. van Veggel, Self-focusing by ostwald ripening: a strategy for layer-by-layer epitaxial growth on upconverting nanocrystals, J. Am. Chem. Soc. 134 (2012) 11068–11071.
[47] F. Zhang, Y. Liu, J. Lei, S. Wang, X. Ji, H. Liu, Q. Yang, Metal-organic-framework-derived carbon nanostructures for site-specific dual-modality photothermal/photodynamic thrombus therapy, Adv. Sci. 6 (2019), 1901378.
[48] Y.F. Wang, G.Y. Liu, L.D. Sun, J.W. Xiao, J.C. Zhou, C.H. Yan, Nd^{3+}-sensitized upconversion nanophosphors: efficient *in vivo* bioimaging probes with minimized heating effect, ACS Nano 7 (2013) 7200–7206.
[49] D.E. Hudson, D.O. Hudson, J.M. Wininger, B.D. Richardson, Penetration of laser light at 808 and 980 nm in bovine tissue samples, Photomed. Laser Surg. 31 (2013) 163–168.
[50] Z. Chen, W. Sun, H.J. Butt, S. Wu, Upconverting-nanoparticle-assisted photochemistry induced by low-intensity near-infrared light: how low can we go? Chemistry 21 (2015) 9165–9170.
[51] C. Li, Z. Hou, Y. Dai, D. Yang, Z. Cheng, P. Ma, J. Lin, A facile fabrication of upconversion luminescent and mesoporous core-shell structured beta-NaYF4:Yb^{3+}, Er^{3+}@$mSiO_2$ nanocomposite spheres for anti-cancer drug delivery and cell imaging, Biomater. Sci. 1 (2013) 213–223.
[52] E. Gkaliagkousi, J. Ritter, A. Ferro, Platelet-derived nitric oxide signaling and regulation, Circ. Res. 101 (2007) 654–662.
[53] J.A. McCleverty, Chemistry of nitric oxide relevant to biology, Chem. Rev. 104 (2004) 403–418.
[54] J. Ye, J. Jiang, Z. Zhou, Z. Weng, Y. Xu, L. Liu, W. Zhang, Y. Yang, J. Luo, X. Wang, Near-infrared light and upconversion nanoparticle defined nitric oxide-based osteoporosis targeting therapy, ACS Nano 15 (2021) 13692–13702.
[55] P. Pacher, J.S. Beckman, L. Liaudet, Nitric oxide and peroxynitrite in health and disease, Physiol. Rev. 87 (2007) 315–424.
[56] H. Yu, S. Yu, H. Qiu, P. Gao, Y. Chen, X. Zhao, Q. Tu, M. Zhou, L. Cai, N. Huang, K. Xiong, Z. Yang, Nitric oxide-generating compound and bio-clickable peptide mimic for synergistically tailoring surface anti-thrombogenic and anti-microbial dual-functions, Bioact. Mater. 6 (2021) 1618–1627.
[57] C. Li, J. Shen, J. Yang, J. Yan, H. Yu, J. Liu, NIR-triggered release of nitric oxide with upconversion nanoparticles inhibits platelet aggregation in blood samples, Part. Part. Syst. Char. 35 (2018), 1700281.
[58] X.S. Fan, L.J. Ke, H.W. Cheng, H. Chen, Z.G. Li, E.Y. Ye, X.J. Loh, Y.L. Wu, G. Liu, Z. B. Li, Enhanced drug retention by anthracene crosslinked nanocomposites for bimodal imaging-guided phototherapy, Nanoscale 13 (2021) 14713–14722.
[59] N.S. Key, C. Negrier, Coagulation factor concentrates: past, present, and future, Lancet 370 (2007) 439–448.